Supporting Information

Vleck et al. 10.1073/pnas.1111333108

SI Methods

Cells. Human melanoma cells and human embryonic lung fibroblasts (HELFs) were propagated in minimal essential media (MEM) supplemented with 10% FBS (Gemini Bio-Products), nonessential amino acids (melanoma cells only) (100 μM; Omega Scientific), and antibiotics (penicillin, 100 U/mL; streptomycin, 100 μg/mL; Invitrogen). HEK-293 cells were propagated in DMEM (Invitrogen) supplemented with 10% FBS and antibiotics. CHO-K1 cells were propagated in F-12K Nutrient Mixture with Kaighn's modification (Invitrogen) supplemented with 10% FBS and antibiotics.

Homology Modeling of Varicella-Zoster Virus Glycoprotein H and Site-Directed Mutagenesis Movie. Individual homology models of varicella-zoster virus (VZV) glycoprotein (g)H were predicted using the known structures for herpes simplex virus (HSV)-2 [Protein Data Bank (PDB) ID code 3M1C], pseudorabies virus (PRV) (PDB ID code 2WQY), and Epstein–Barr virus (EBV) (PDB ID code 3PHF) gH (1–3) with DeepView/Swiss Pdb-Viewer to submit amino acid alignments to SWISS-MODEL (4) via the ExPASy web server (http://swissmodel.expasy.org). The methods that SWISS-MODEL uses for structure prediction have been described previously, providing information on the modeling program (ProModII), energy minimization (Gromos force field), and model assessment (ANOLEA mean force potential) used to generate the homology models (5). To validate the homology model structures, Ramachandran plots were generated from the PDB files produced by SWISS-MODEL using the PDBSum web server (6) (http://www.ebi.ac.uk/pdbsum). All molecular visualizations were generated using Visual molecular dynamics (7) and POV-Ray (Persistence of Vision Raytracer). The gH movie showing the locations of site-directed mutagenesis was produced by compiling ray-traced images using Adobe Premiere Pro.

Primers Used for the Mutagenesis and Cloning of ORF37[gH] and ORF60[gL]. See Table S3 for a complete list of primers.

VZV ORF37[gH] Mutagenesis in pOka Cosmids. The mutations S42A, N45A, S47A, S47T, T351A, and T751A were introduced into the VZV genome using cosmid vectors as previously described with modifications specific for ORF37[gH] (8). The complete genome of the VZV parental Oka strain (pOka) is contained in five overlapping SuperCos 1 cosmid vectors (Stratagene) designated pFsp73 (nucleotides 1–33128), pSpe14 (nucleotides 21795–61868), pAfl17 (nucleotides 53828–79886), pAvr102 (nucleotides 72298–96113), and pSpe23ΔAvrII (nucleotides 94055–125123) (9). ORF37 (nucleotides 65935–66861) is located within the pAfl17 cosmid. A KpnI fragment of ∼15.5 kb (nucleotides 57343–72902) containing the ORF37 sequence was cloned into the pNEB193 plasmid (New England BioLabs). In this plasmid, designated pNEB193/pAfl-KpnI, the unique SpeI (nucleotide 5010) and SgrAI (nucleotide 15853) sites, located 4,067 nt upstream and 6,776 nt downstream of the ORF37 ATG, respectively, were used to insert the ORF37 mutations into the cosmid. The pNEB193/pAfl-KpnI plasmid contained unique BbvCI (nucleotide 7387) and Bsu36I (nucleotide 13361) sites, located 1,690 nt upstream and 4,281 nt downstream of the ORF37 ATG, respectively. The pNEB193/pAfl-KpnI plasmid was used as a template for PCR-based mutagenesis. PCR mutagenesis was performed as previously described, with two steps of PCR to introduce the appropriate mutation into the BbvCI-Bsu36I fragment (10). Briefly, two PCR steps were performed using a 5′ outside forward primer (2149-gH[37]-F) in combination with an internal mutagenic reverse primer or a 3′ outside reverse primer (gH[37]4519-R) with an internal mutagenic forward primer. In the second step, the two PCR products were combined and used as template for the second PCR to generate a 6.67-kb fragment containing the mutation. This fragment was cloned into pCR4-TOPO-TA (Invitrogen) and fully sequenced to verify that only the expected mutation was present. An unexpected second mutation, T127A, was identified in the pCR4-TOPO-TA-gH-S47A sequence. The two mutations were separated using restriction enzyme sites within ORF37[gH] to create two individual gH mutants, pCR4-TOPO-TA-gH-S47A and pCR4-TOPO-TA-gH-T127A. The pCR4-TOPO-TA-gH plasmids containing the 6.67-kb fragment with the specific substitutions were digested with BbvCI and Bsu36I, and the fragment was inserted into pNEB193/pAfl-KpnI, replacing the wild-type BbvCI-Bsu36I fragment. The pNEB193/pAfl-KpnI mutant plasmids were then digested with SpeI and SgrAI and inserted into the pAfl17 cosmid, replacing the wild-type SpeI-SgrAI fragment (nucleotides 61941–72784 in pOka). These cosmids were sequenced to verify the mutations.

VZV ORF37[gH] Mutagenesis in pOka-DX Bacterial Artificial Chromosomes. Mutagenesis of αX, α8, α9, α12, α14, and FPNG was performed using the self-excisable pOka-DX BAC as described previously with modifications specific for ORF37[gH] (11). Briefly, mutagenesis primers for recombination were used to amplify the Kan^r gene from the pKANS vector using AccuPrime Pfx (Invitrogen). The PCR products were cloned into pCR4-TOPO-TA after the addition of adenosine overhangs using recombinant Taq (Invitrogen). Clones were sequenced to determine that the VZV-specific sequences did not have any unexpected deletions or substitutions. The Kan^r cassette flanked with the VZV sequences was amplified from the pCR4.0 vectors using short primers to generate high yields of PCR product, which were gel-purified (Qiagen), and then 100 ng was used for recombination. After the red recombination steps to insert the mutations and remove the Kan^r cassette, BACs were purified using a Large-Construct Kit (Qiagen). All purified BACs were digested with HindIII to ensure the expected DNA fragments were present. In addition, BACs were sequenced directly across the sites of mutagenesis to ensure that unexpected deletions or substitutions were not present.

All of the cysteine mutants and the S694F/C724A mutant were generated using the pOka-DX BAC with a modification to expedite mutagenesis. A pOka-DX-ΔORF37 BAC was generated by red recombination as described in the previous section using the primers [D37]F65895–65915 and [D37]R68477–68497. A wild-type ORF37 construct was generated, pORF37-Kan^r, consisting of two regions of the pOka genome (nucleotides 65824–67237 and 67016–68542; nucleotide locations were determined from the pOka-DX BAC) that flanked the Kan^r cassette. This contained ORF37 coding for amino acids 1–434 and 362–841 of gH plus 111 nucleotides upstream and 82 nucleotides downstream of the ORF. The ORF37-Kan^r cassette was cloned into pCR4-TOPO-TA and flanked by the PmeI restriction endonuclease site. To generate the C327A, C540A, C575A, C647A, C793A, C724A, C727A, and S694F/C724A mutants, site-directed mutagenesis of ORF37 was performed by PCR using pORF37-Kan^r and the appropriate mutagenesis primers. All of the vectors were sequenced to determine that the expected mutations were present. The restriction endonucleases NaeI and

PmeI were used to digest 5 μg of pORF37-Kan^r generating 20-, 1,499-, 2,445-, and 3,951-bp DNA fragments. The 3,951-bp fragment was gel-purified and used for red recombination as previously described.

To repair the lethal VZV gH substitutions, pOka-DX BACs carrying the ORF37 mutations had their complete ORF deleted by red recombination as described in the previous section using the primers [D37]F65895–65915 and [D37]R68477–68497 and replaced by the WT pORF37-Kan^r by red recombination. BACs were sequenced to confirm the WT ORF37 sequence, and purified BACs were used to recover infectious virus as described previously.

Construction of Expression Plasmids Containing ORF37[gH] and ORF60 [gL]. The WT ORF37[gH], mutant ORF37[gH]s, and WT ORF60 [gL] were cloned into pCR4.0 and the mammalian expression vector pCDNA3.1 (Invitrogen). Initially, pCR4.0 constructs for WT ORF37, ORF60, and ORF37 with the mutations S42A, N45A, S47A, S47T, T127A, T351A, or T751A were generated from the cosmid by PCR using AccuPrime Pfx and TOPO-TA cloning (Invitrogen) and the appropriate primers that inserted a HindIII site and a Kozak sequence immediately before the initiation codon plus an additional termination codon and an XhoI site after the ORF. HindIII and XhoI were used to transfer the cloned PCR products from the pCR4.0 vector into pCDNA3.1. All vectors were sequenced to confirm that the gH and gL sequences did not contain any unexpected deletions or substitutions.

Site-directed PCR-based mutagenesis was used to create pCDNA3.1-gH vectors containing the mutations αX, C327A, α8, α9, α12, α14, C540A, C575A, C647A, S694F, C703A, C724A, C727A, or FPNG. Phosphorylated, adjoining mutagenesis primers and primers that included unique restriction endonuclease sites were used to amplify the gH mutants from the WT pCR4-gH vector. PCR products were inserted into the pCDNA3.1-gH vector using unique restriction endonucleases. The double mutants S694F/C724A and S694F/C727A were generated using pCDNA3.1-gH [C724A] or -gH[C727A] DNA as the template and primers that inserted the S694F substitution. All vectors were sequenced to verify the presence of the expected mutation.

The pME18S-gH-TL vector was a kind gift from Tadahiro Suenaga and Hisashi Arase (Osaka University, Osaka, Japan) (12). This vector contains a stop codon in place of E834, and was used in the cell fusion assay and analysis of surface expression in CHO-K1 cells used in the fusion assay. All gH mutations were inserted from the pCDNA3.1-gH vectors into the pME18S-gH-TL vector using unique restriction endonucleases. At least two independent clones for each vector were generated, and all vectors were sequenced to verify the presence of the expected mutation.

Generation of Recombinant Viruses. Recombinant viruses were isolated by transfection of human melanoma cells with mutant cosmids and the four wild-type cosmids or with BAC DNA as previously described (8). At least two clones for each mutant were transfected. Virus was typically recovered 5–10 d post-transfection. DNA was isolated from infected cells using DNAzol according to the manufacturer's instructions (Invitrogen) or using phenol-chloroform. PCR and sequencing were performed to confirm that the expected mutations were present. BAC-derived recombinant viruses were passed in HELFs until the MiniF$^-$ sequences *Cat* (P1/P2; see primers) and *SopA* (P3/P4; see primers) were not detectable by PCR, as previously described (11). In addition, the primers gH[37]980-F and gH[37]1395-R were used to detect ORF37 to determine the presence of virus.

Transfection of Expression Vectors. Cells were transfected with a total of 0.5 μg DNA per cm^2 with Lipofectamine 2000 according to the manufacturer's instructions (Invitrogen). Cells transfected with multiple plasmids were transfected with equimolar amounts of each plasmid. The control "gH only" represents cells transfected with the gH plasmid and the empty vector in place of the gL plasmid. At 48 h posttransfection, cells were either fixed with PBS plus 4% paraformaldehyde or lysed in extraction buffer [0.1 M Tris-base (pH 7.2), 0.1 M NaCl, 5 mM KCl, 1 mM $CaCl_2$, 0.5 mM $MgCl_2$, 1% sodium deoxycholate, 1% Nonidet P-40 plus an EDTA-free protease inhibitor mixture (Roche) (13)].

Confocal Microscopy of Infected and Transfected Cells. At 48 h postinfection or posttransfection, cells were fixed in 4% paraformaldehyde and blocked with PBS plus 10% donkey serum. To permeabilize cells, blocking and staining solutions contained 0.1% Triton-X. Confocal microscopy of VZV gH was performed using the anti-gH mAb SG3 (Meridian Life Science). pOka and αX gH confocal microscopy was also performed using the conformation-dependent, complement-independent neutralizing antibodies mAb 206 and mAb 258 (kind gifts of Charles Grose, University of Iowa, Iowa City, IA) (14). Primary antibodies were used to detect virus protein gE (rabbit polyclonal) (15) and cellular protein trans-Golgi network (TGN) 46 (AHP500 polyclonal sheep anti-TGN46; AbD Serotec). Secondary antibodies used were FITC-coupled donkey anti-sheep (Jackson ImmunoResearch), Alexa Fluor 488 donkey anti-mouse (Invitrogen), Alexa Fluor 547 donkey anti-rabbit (Invitrogen), Alexa Fluor 555 donkey anti-mouse (Invitrogen), Alexa Fluor 647 donkey anti-rabbit (Invitrogen), Alexa Fluor 647 donkey anti-sheep (Invitrogen), and Hoechst 33342 (Invitrogen). Confocal microscopy was performed using a Zeiss LSM510 confocal microscope equipped with two-photon excitation.

Immunoprecipitation and Western Blot Analysis of gH. Immunoprecipitation of gH from lysates of infected or transfected cells was performed as previously described (16). Briefly, the SG3 monoclonal antibody to gH (Meridian Life Science) or no antibody was cross-linked to immobilized protein G (Protein G Plus UltraLink Resin; Thermo Scientific). Lysates were incubated with bound antibodies overnight, washed extensively, and eluted with SDS sample buffer by incubating the beads at 100 °C for 5 min. Denatured samples were resolved on SDS/polyacrylamide gels. Proteins were transferred to Immobilon-P membranes (Millipore Bioscience) and blocked with 5% BSA (mouse monoclonal antibodies) or dried milk (rabbit polyclonal antibodies). gH was detected using two primary antibodies: mouse mAb SG3 anti-gH or the rabbit polyclonal antibody designated $gH_{292–305}$. The $gH_{292–305}$ antibody was produced by GenScript as a rabbit antisera against a synthetic peptide composed of gH amino acids 292–305.

Western blots of virus lysates were performed to control for levels of virus protein expression. Membranes were probed for gE (mouse mAb 8612 anti-gE; Millipore), IE63 (rabbit anti-IE63; a kind gift of William Ruyechan, State University of New York, University at Buffalo, Buffalo, NY), ORF23 (rabbit) (17), and cellular α-tubulin (clone B-5-1-2 mouse anti-α-tubulin; Sigma). All primary antibodies were detected using horseradish peroxidase-conjugated antibodies to anti-mouse or anti-rabbit IgG and an ECL Plus Detection Kit (GE Healthcare Bio-Sciences).

Virus Titration, Replication Kinetics, and Plaque Sizes. Virus titration was performed by 10-fold serial dilution on melanoma cells, done in triplicate. For replication kinetics, 1×10^6 melanoma cells were seeded in six-well plates 24 h before inoculation with $\log_{10}$ 3.0 PFU of virus. Virus was harvested and titered in triplicate on melanoma cells every 24 h. All titer plates were fixed at 3 d postinfection (dpi) in 4% paraformaldehyde, and immunohistochemistry was performed with an anti-VZV polyclonal serum or a mixture of mouse monoclonal antibodies to VZV (Meridian Life Science). Images of stained plaques ($n = 30$) were digitally

captured, and the plaques were outlined using ImageJ (18) to calculate the area (mm^2).

Virus Neutralization Assay. Neutralization assays were performed as previously described (19). Briefly, 1×10^6 HELF cells were seeded in six-well plates 24 h before inoculation. Monolayers were inoculated with $\log_{10}$ 3.0 PFU pOka or αX for 90 min at 37 °C. Media were changed, and then 25 μg of anti-gH mAb 206 or SG3 was added and repeated at 24-h intervals. Mock-treated cells received only media. Cells were fixed at 96 h postinfection in 4% paraformaldehyde and stained with anti-VZV polyclonal serum. For neutralization of pOka and αX by mAb 206, cells were seeded, infected, and treated as above, and virus was harvested every 24 h for 96 h and titered as above.

Virulence of gH Mutant Viruses in Human Skin Xenografts. Skin xenografts were prepared in homozygous CB-$17^{scid/scid}$ mice using human fetal skin tissue obtained according to federal and state regulations as previously described (20). Animal protocols complied with the Animal Welfare Act and were approved by the Stanford University Administrative Panel on Laboratory Animal Care. Human tissues were obtained, in accordance with state and federal regulations, from Advanced Bioscience Resources. VZV-infected HELFs were used to inoculate the xenografts. All virus inoculum titers were statistically equivalent. Skin xenografts were harvested at 10 and 21 dpi. Half of each xenograft was homogenized and resuspended in 1 mL PBS for virus titration and DNA extraction for PCR, and ORF37 was sequenced to confirm that the expected mutation was present.

T-Cell Entry Assay. Primary human tonsil tissue was obtained according to a protocol approved by the Stanford University Committee for Research Involving Human Subjects, and T cells were extracted as previously described (21). Infected HELF monolayers were overlaid with 2×10^7 T cells. Uninfected HELFs overlaid with T cells were used as a negative control. The titer of infected HELFs at the time of T-cell overlay was determined by titering duplicate flasks on melanoma cells. T cells were harvested at 24 h postinfection and fixed and stained using the Cytofix/Cytoperm Fixation/Permeabilization Kit (BD Biosciences) following the manufacturer's recommended protocol. Cells were stained for gE (mouse mAb 8612 anti-gE; Millipore) and CD3 conjugated to phycoerythrin or the isotype control (BD Biosciences). gE was detected using Alexa Fluor 647 (Invitrogen). Cells were analyzed using a FACSCalibur controlled by CellQuest Pro (BD Biosciences). Background based on isotype control staining was subtracted from each sample. T-cell infection was normalized to virus titer in HELF cells at the time of T-cell overlay.

Retroviral Production of Cell Lines Used for the Cell Fusion Assay. The MFG Lox-dsRed-Lox-GFP (LDL-GFP) and pBABe-Cre-puro retroviral vectors have been previously described (22, 23). Retroviruses were produced by FuGene6 (Roche)-mediated transfection of 293-T cells at 70% confluence in a 10-cm dish cultured in DMEM (Invitrogen) supplemented with 10% FBS. Retroviral vector plasmid (4 μg) was cotransfected with pCL-Eco (4 μg) and VSVg (0.4 μg). Supernatants were collected 48 and 72 h posttransfection, filtered through a 0.45-μm filter, and used directly for infection of CHO-K1 or melanoma cells, supplemented with polybrene (8 μg/mL). Cells were transduced overnight and media were changed the next day. Puromycin selection (8 μg/mL) of CHO-K1-Cre cells was started 48 h posttransduction. LDL-GFP-transduced melanoma cells were allowed to expand, and red fluorescent cells were sorted by FACS on a modified Digital FACStar running Diva hardware and software (BD Biosciences).

Quantification of gH Cell Surface Expression by Flow Cytometry. CHO-K1 cells were transfected with WT or mutant expression constructs in pME18S-gH-TL or pCDNA-gH in combination with pCDNA-gL using Lipofectamine 2000. Cells were dislodged at 24 h posttransfection using an enzyme-free cell dissociation buffer (Invitrogen) and resuspended in FACS staining buffer [DPBS (Dulbecco's Phosphate-Buffered Saline) with 0.2% IgG-free BSA and 0.1% NaN_3] for cell surface staining with anti-VZV gH mAbs SG3 (Meridian Life Science), 206, and 258. An anti-mouse IgG-Alexa Fluor 488 antibody (Invitrogen) was used to detect anti-VZV gH antibodies. Stained cells were fixed with 1% paraformaldehyde and then analyzed using a FACSCalibur controlled by CellQuest Pro (BD Biosciences). FlowJo (Tree Star) was used to determine the levels of gH surface expression. Experiments were performed with at least two gH mutant clones, each done in duplicate.

Quantitative Cell Fusion Assay. CHO-K1 cells constitutively expressing Cre recombinase were transfected with equal quantities of WT or mutant pME18S-gH-TL expression constructs in combination with pCAGGS-gB and pCDNA-gL using Lipofectamine 2000. At 6 h posttransfection, CHO-K1 Cre cells were trypsinized and mixed with LDL-GFP melanoma cells constitutively expressing DsRed from the Lox-DsRed-Lox-GFP cassette. Upon CHO-K1–melanoma cell fusion, Cre induces recombination of the Lox-DsRed-Lox-GFP cassette, enabling GFP expression. At 36 h postseeding, cells were trypsinized, resuspended in FACS buffer (PBS with 2.5% FBS and 2 mM EDTA), and analyzed on a modified Digital FACStar running Diva hardware and software (BD Biosciences). The frequency of GFP-positive cells was determined using FlowJo, enabling the direct quantification of fusion events for the gH mutants, which were normalized to WT gH. A negative control where gB was omitted from the transfection was used to establish background levels of GFP-positive cells and subtracted from each of the samples including the gB/gH/gL-positive control. The pCAGGS-VZV-gB vector was a kind gift from Tadahiro Suenaga and Hisashi Arase (Osaka University, Osaka, Japan) (12). Experiments were performed with at least two gH mutant clones, each done in duplicate.

Circular Dichroism. WT α9 (^{388}FLLDEIVDVQYQLKFLNYILMR^{409}), mutant α9 (^{388}FLLDEIVDVQYAAKFLNYILMR^{409}), WT α12 (^{447}ANVDYFISYDEARDQLKTAYAL^{468}), and mutant α12 (^{447}ANVDYFISYAAARDQAKTAYAL^{468}) at a purity of >98%, as determined by mass spectrometry and HPLC, were purchased from GenScript. Peptides were dissolved in 10 mM sodium phosphate buffer (pH 7.0). Peptide concentration was calculated using the extinction coefficient 2,980 $M^{-1}cm^{-1}$ for α9 and 4,470 $M^{-1}cm^{-1}$ for α12, determined using ProtParam on the ExPASy web server (http://web.expasy.org/protparam). CD spectra were acquired on an Aviv 62DS instrument (Aviv Biomedical) with a 1-mm path-length cell. Measurements were taken every 1 nm at 0 °C with a 10-s averaging time and a peptide concentration of 100 μM in buffer with increasing percentages of trifluoroethanol (TFE). Mean residue ellipticity was calculated as $\theta \times MRW/[peptide]$, where θ is absorbance corrected for background, MRW is average molecular weight per residue, and peptide concentration is in mg/mL.

Statistical Analyses. Statistical analyses were performed using GraphPad Prism version 5.0a for Windows (GraphPad Software). Student's *t* test was used to analyze T-cell entry. One-way ANOVA was used to analyze plaque size, cell fusion, and cell surface expression for the cell fusion assay and cell surface expression for confocal microscopy. Two-way ANOVA was used to analyze in vitro replication kinetics, in vivo skin xenograft replication, antibody detection of pOka and αX, and in vitro neutralization replication kinetics of pOka and αX treated with mAb 206. For all statistics, $^*P < 0.05$, $^{**}P < 0.01$, $^{***}P < 0.001$.

1. Matsuura H, Kirschner AN, Longnecker R, Jardetzky TS (2010) Crystal structure of the Epstein-Barr virus (EBV) glycoprotein H/glycoprotein L (gH/gL) complex. *Proc Natl Acad Sci USA* 107:22641–22646.
2. Backovic M, et al. (2010) Structure of a core fragment of glycoprotein H from pseudorabies virus in complex with antibody. *Proc Natl Acad Sci USA* 107:22635–22640.
3. Chowdary TK, et al. (2010) Crystal structure of the conserved herpesvirus fusion regulator complex gH-gL. *Nat Struct Mol Biol* 17:882–888.
4. Arnold K, Bordoli L, Kopp J, Schwede T (2006) The SWISS-MODEL workspace: A web-based environment for protein structure homology modelling. *Bioinformatics* 22: 195–201.
5. Kiefer F, Arnold K, Künzli M, Bordoli L, Schwede T (2009) The SWISS-MODEL Repository and associated resources. *Nucleic Acids Res* 37(Database issue):D387–D392.
6. Laskowski RA (2009) PDBsum new things. *Nucleic Acids Res* 37(Database issue): D355–D359.
7. Humphrey W, Dalke A, Schulten K (1996) VMD: Visual molecular dynamics. *J Mol Graph* 14:33–38.
8. Mallory S, Sommer M, Arvin AM (1997) Mutational analysis of the role of glycoprotein I in varicella-zoster virus replication and its effects on glycoprotein E conformation and trafficking. *J Virol* 71:8279–8288.
9. Niizuma T, et al. (2003) Construction of varicella-zoster virus recombinants from parent Oka cosmids and demonstration that ORF65 protein is dispensable for infection of human skin and T cells in the SCID-hu mouse model. *J Virol* 77:6062–6065.
10. Baiker A, et al. (2004) The immediate-early 63 protein of varicella-zoster virus: Analysis of functional domains required for replication in vitro and for T-cell and skin tropism in the SCIDhu model in vivo. *J Virol* 78:1181–1194.
11. Tischer BK, et al. (2007) A self-excisable infectious bacterial artificial chromosome clone of varicella-zoster virus allows analysis of the essential tegument protein encoded by ORF9. *J Virol* 81:13200–13208.
12. Suenaga T, et al. (2010) Myelin-associated glycoprotein mediates membrane fusion and entry of neurotropic herpesviruses. *Proc Natl Acad Sci USA* 107:866–871.
13. Grose C, Edwards DP, Weigle KA, Friedrichs WE, McGuire WL (1984) Varicella-zoster virus-specific gp140: A highly immunogenic and disulfide-linked structural glycoprotein. *Virology* 132:138–146.
14. Montalvo EA, Grose C (1986) Neutralization epitope of varicella zoster virus on native viral glycoprotein gp118 (VZV glycoprotein gpIII). *Virology* 149:230–241.
15. Ito H, et al. (2005) Role of the varicella-zoster virus gene product encoded by open reading frame 35 in viral replication in vitro and in differentiated human skin and T cells in vivo. *J Virol* 79:4819–4827.
16. Oliver SL, et al. (2009) Mutagenesis of varicella-zoster virus glycoprotein B: Putative fusion loop residues are essential for viral replication, and the furin cleavage motif contributes to pathogenesis in skin tissue in vivo. *J Virol* 83:7495–7506.
17. Chaudhuri V, Sommer M, Rajamani J, Zerboni L, Arvin AM (2008) Functions of varicella-zoster virus ORF23 capsid protein in viral replication and the pathogenesis of skin infection. *J Virol* 82:10231–10246.
18. Abramoff MD, Magelhaes PJ, Ram SJ (2004) Image processing with ImageJ. *Biophotonics Int* 11:36–42.
19. Vleck SE, et al. (2010) Anti-glycoprotein H antibody impairs the pathogenicity of varicella-zoster virus in skin xenografts in the SCID mouse model. *J Virol* 84: 141–152.
20. Moffat JF, Stein MD, Kaneshima H, Arvin AM (1995) Tropism of varicella-zoster virus for human $CD4^+$ and $CD8^+$ T lymphocytes and epidermal cells in SCID-hu mice. *J Virol* 69:5236–5242.
21. Berarducci B, et al. (2010) Functions of the unique N-terminal region of glycoprotein E in the pathogenesis of varicella-zoster virus infection. *Proc Natl Acad Sci USA* 107: 282–287.
22. Koshy AA, et al. (2010) Toxoplasma secreting Cre recombinase for analysis of host-parasite interactions. *Nat Methods* 7:307–309.
23. Krempler A, Henry MD, Triplett AA, Wagner KU (2002) Targeted deletion of the Tsg101 gene results in cell cycle arrest at G1/S and p53-independent cell death. *J Biol Chem* 277:43216–43223.

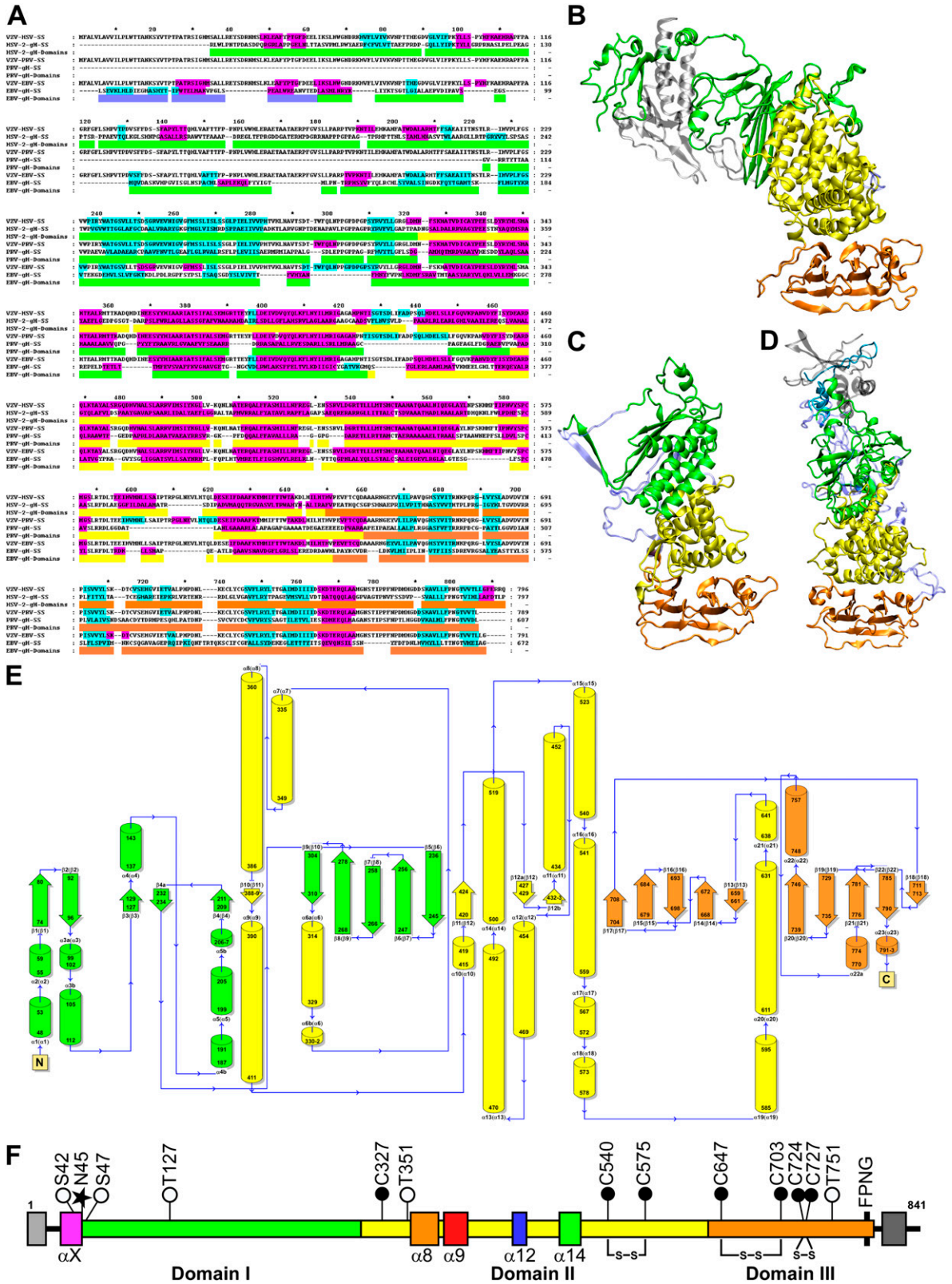

Fig. S1. Homology modeling of VZV gH based on the structures of HSV-2, PRV, and EBV gH. (*A*) Amino acid alignments used to generate the VZV gH homology models derived from HSV, PRV, or EBV (*B–D*). The secondary structures (SS) of gH for the VZV homology models and those derived from the X-ray crystallography data for HSV, PRV, and EBV are shaded to show α-helices (pink) and β-sheets (cyan). The gH domains of HSV-2, PRV, and EBV are shaded in accordance with the criteria for the crystallography studies. HSV-2: DI (green), DII (yellow), and DIII (orange). PRV and EBV: DI (mauve), DII (green), DIII (yellow), and DIV (orange). (*B–D*) Homology models of VZV gH based on HSV-2 (*B*), PRV (*C*), and EBV gH (*D*). Domains in the models are shaded in accordance with the amino acid alignments (*A*). HSV-2: DI (green), DII (yellow), and DIII (orange). PRV and EBV: DI (cyan), DII (green), DIII (yellow), and DIV (orange). Light blue designates gaps of five amino acids or greater that occur in the sequence alignment (*A*). HSV-2 gL is shown in silver and EBV gL is shown in dark gray. (*E*) A

Legend continued on following page

topology diagram of VZV gH modeled on HSV gH. Cylinders indicate α-helices. Arrows indicate β-sheets. α-Helices and β-sheets are numbered according to the VZV prediction. Numbers shown in parentheses are in accordance with the HSV-2 gH structure, and are used throughout the text. Residues are indicated in each α-helix or β-sheet. (*F*) Linear diagram of gH depicting targeted mutations. Signal sequence, light gray box; DI, green; DII, yellow; DIII, orange; αX, pink box; serine and threonine, white circles; glycosylation site, black star; cysteines, black circles; α8, orange box; α9, red box; α12, blue box; α14, green box; FPNG, black bar; transmembrane region, dark gray box. Predicted disulfide bonds are connected with lines.

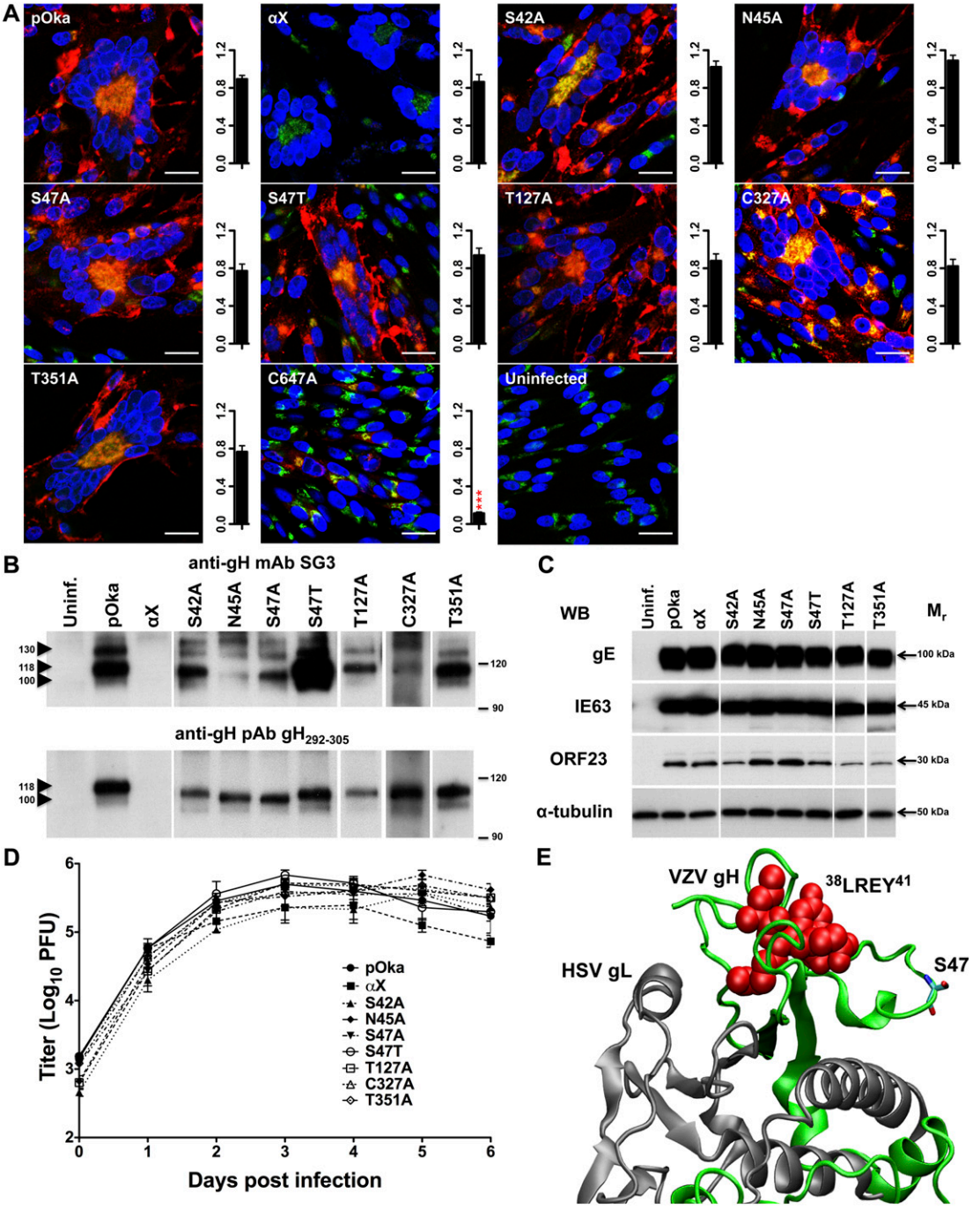

Fig. S2. Localization, maturation, and in vitro replication of gH DI mutants. (*A*) Confocal microscopy and plaque size (mm^2) of pOka and all mutant viruses in infected cells. gH, red; TGN, green; nuclei, blue. (Scale bars, 25 μm.) (*B*) Anti-gH SG3 and $gH_{292–305}$ Western blot of gH immunoprecipitated from infected cells. Arrowheads on the left indicate gH protein species with specified calculated molecular masses of 100 kDa (immature gH), 118 kDa (mature gH), and 130 kDa (a previously unidentified form of gH likely representing further gH modification). Calculated molecular masses are based on the standard protein ladder indicated on the right. (*C*) Western blots (WB) of lysates from cells infected with pOka and DI mutant viruses for gE, IE63, ORF23, and α-tubulin. Molecular masses are indicated on the right. (*D*) In vitro replication kinetics. (*E*) VZV gH DI showing the αX residues ^{38}LREY^{41} in red space fill and the S47 residue in stick form with nitrogen in blue and oxygen in red. Note the outward-pointing hydroxyl on the S47 residue. HSV gL is shown in gray. Mean ± SEM. ***$P < 0.001$.

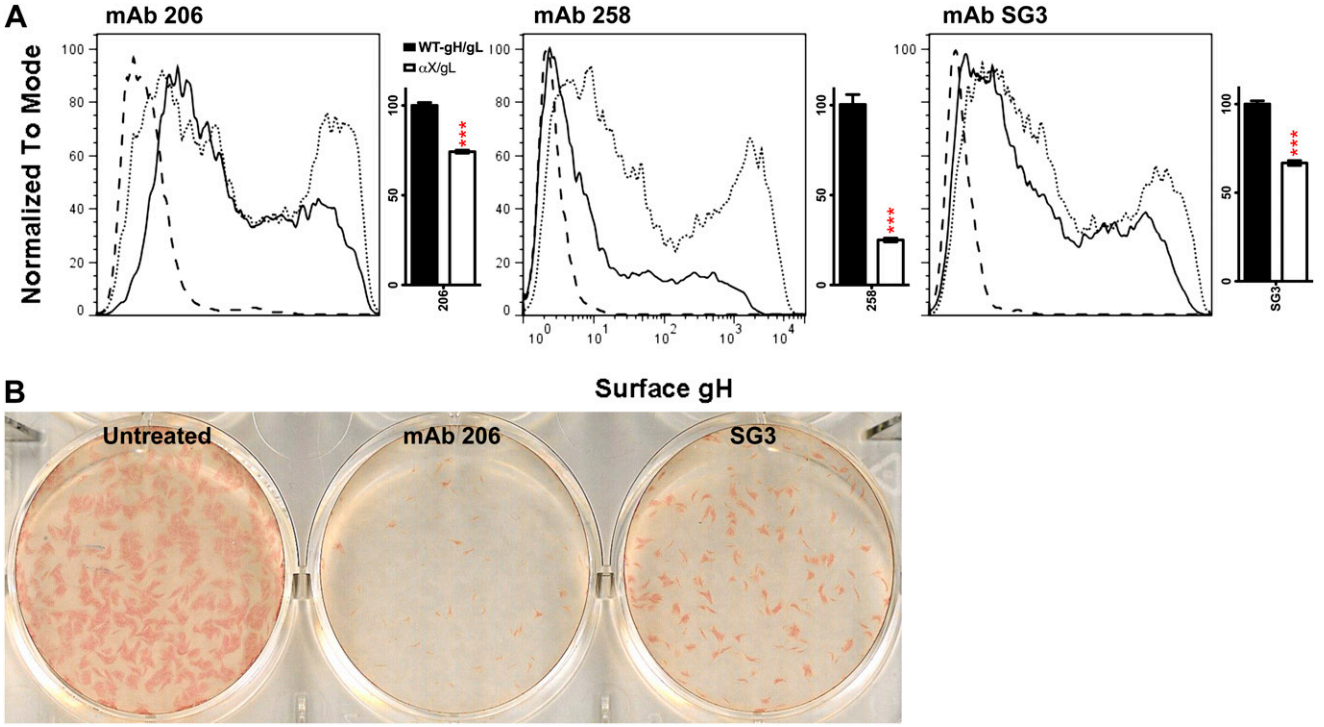

Fig. S3. Altered αX detection by neutralizing antibodies in transfected cells. (*A*) Cell surface expression of gH (dotted line, black bar), αX (black line, white bar), or gH only (dashed line) in transfected cells. Quantification is shown on the right. Mean ± SEM. ***$P < 0.001$. (*B*) Neutralization of pOka by mAb 206 and SG3, demonstrating that SG3 is a neutralizing antibody.

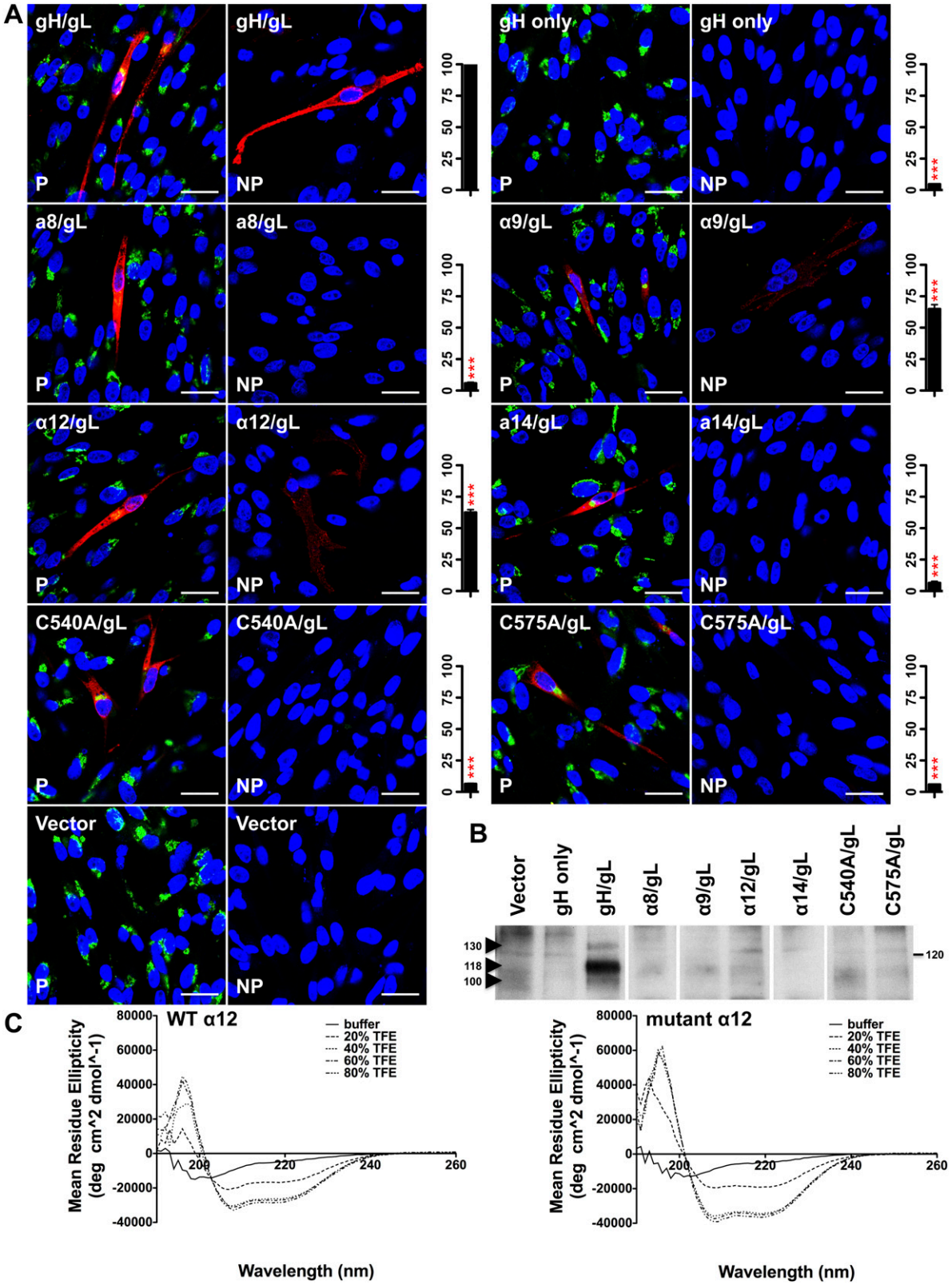

Fig. S4. Localization and maturation of gH DII mutants and structural analysis of α12. (*A*) Confocal microscopy and cell surface expression (% of WT) of gH and DII lethal mutants in transfected cells. NP, nonpermeabilized; P, permeabilized; gH, red; TGN, green; nuclei, blue. (Scale bars, 25 μm.) Mean ± SEM. ***$P <$ 0.001. (*B*) Anti-gH SG3 Western blot of gH immunoprecipitated from transfected cells. Arrowheads on the left indicate gH protein species with specified calculated molecular masses of 100 kDa (immature gH), 118 kDa (mature gH), and 130 kDa (a previously unidentified form of gH likely representing further gH modification). Calculated molecular masses are based on the standard protein ladder indicated on the right. (*C*) Circular dichroism spectra of mimetic peptides of WT α12 and mutant α12 in buffer and increasing concentrations of TFE.

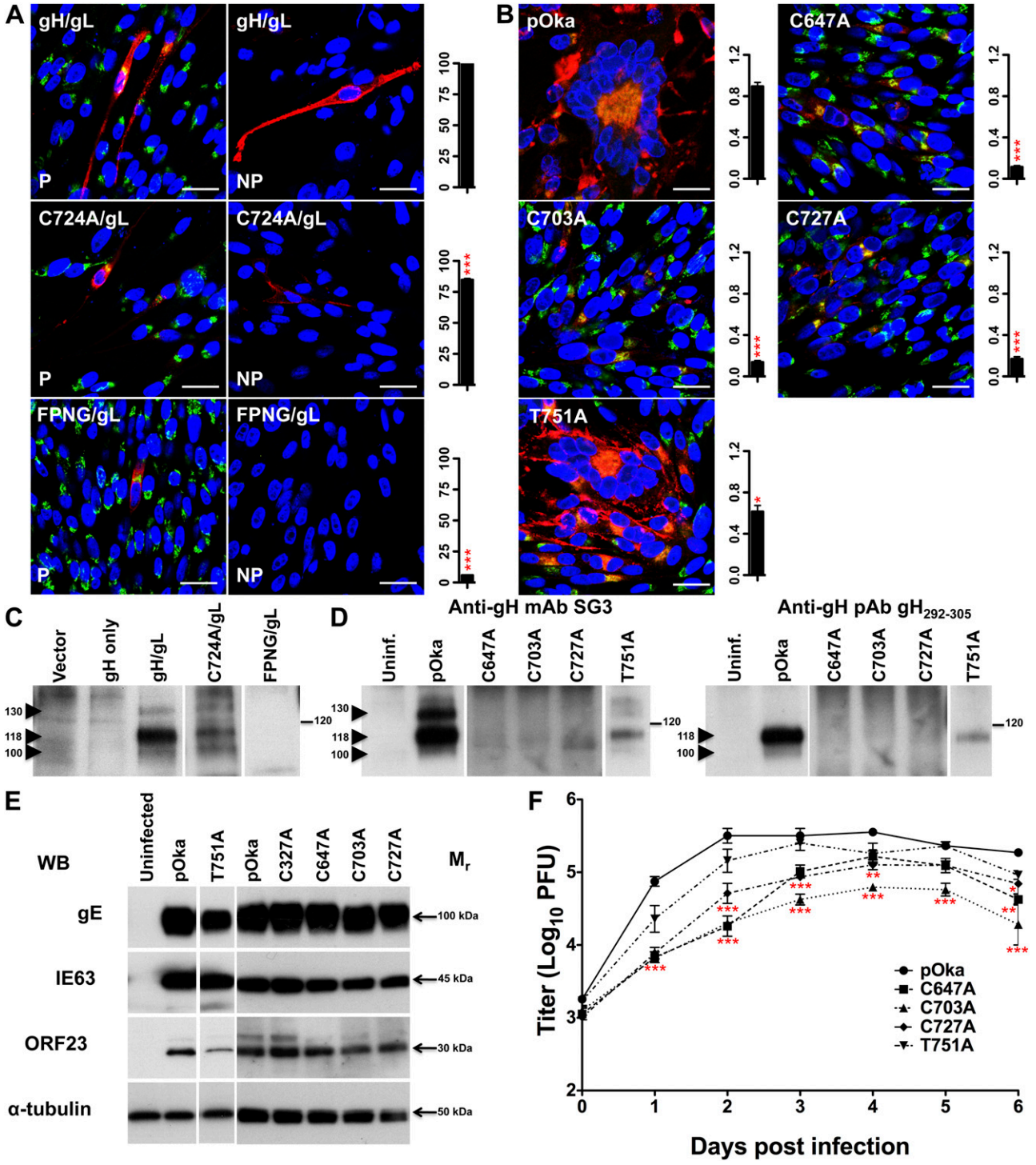

Fig. S5. Localization, maturation, and in vitro replication of gH DIII mutants. (*A*) Confocal microscopy and cell surface expression (% of WT) of C724A and FPNG in transfected cells. NP, nonpermeabilized; P, permeabilized. (*B*) Confocal microscopy and plaque size (mm^2) of pOka, C647A, C703A, C727A, and T751A in infected cells. gH, red; TGN, green; nuclei, blue. (Scale bars, 25 μm.) (*C* and *D*) Anti-gH SG3 and $gH_{292–305}$ (*D* only) Western blot of gH immunoprecipitated from (*C*) transfected or (*D*) infected cells. Arrowheads on the left indicate gH protein species with specified calculated molecular masses of 100 kDa (immature gH), 118 kDa (mature gH), and 130 kDa (a previously unidentified form of gH likely representing further gH modification). Calculated molecular masses are based on the standard protein ladder indicated on the right. (*E*) Western blots of lysates from cells infected with pOka and DIII mutant viruses for gE, IE63, ORF23, and α-tubulin. Molecular masses are indicated on the right. (*F*) In vitro replication kinetics. Mean ± SEM. $*P < 0.05$, $**P < 0.01$, $***P < 0.001$.

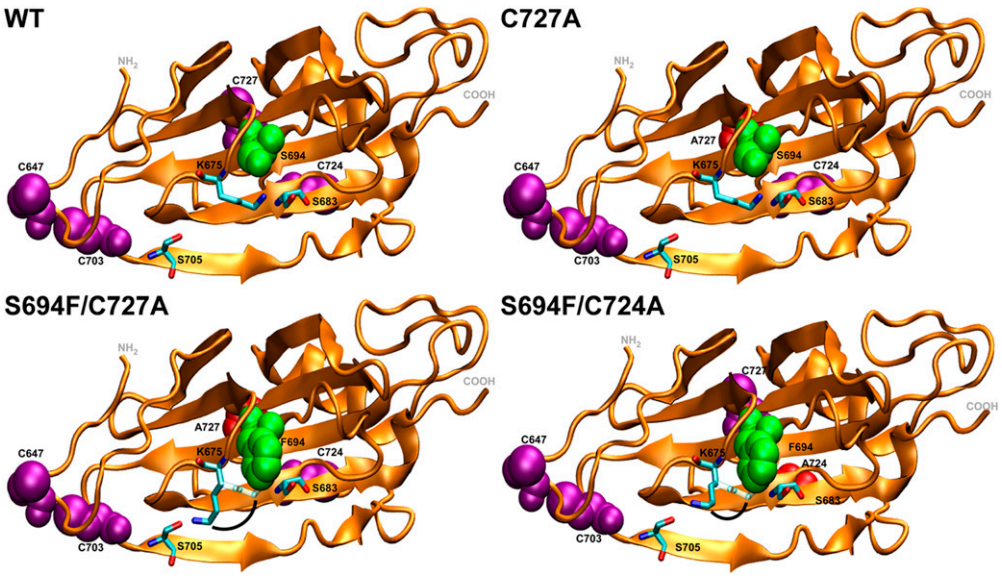

Fig. S6. The S694F mutation is predicted to distort VZV gH DIII. Homology models of DIII for WT gH and the mutants C727A, S694F/C727A, and S694F/C724A. Cysteines, purple; S694F, green; alanine substitutions, red. Residues K675, S683, and S705 are represented in stick form (nitrogen, blue; oxygen, red). The black line depicts predicted movement of the K675 in the compensatory mutants S69F/C727A and S694F/C724A.

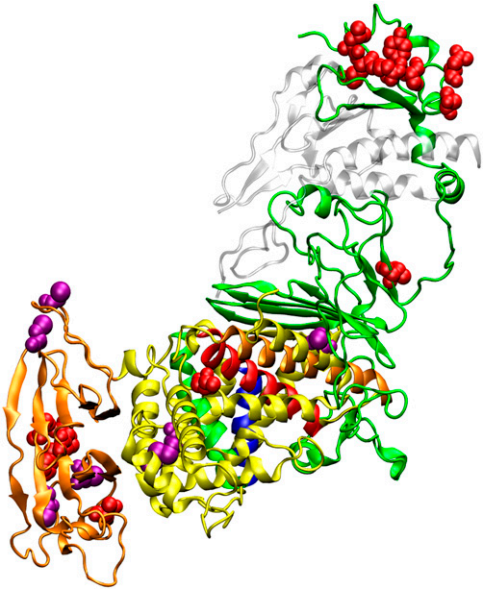

Movie S1. A movie to enable visualization of VZV mutants used to study gH function. The movie time line is as follows: 0–3 s, domain (D)II and DIII fade out; 3–13 s, ^{38}LREY^{41} (αX), S42, N45, S47, and T127 appear sequentially in red space fill; 13–18 s, DI rotates about the *y* axis; 18–27 s, DII and DIII fade in, then DI and DIII fade out; 28–33 s, DII, with α-helices 8 (orange), 9 (red), 12 (blue), and 14 (green), orientates to the position shown in Fig. 1; 33–41 s, T351, C327, C540, and C575 appear sequentially in red and purple space fill; 41–52 s, DII rotates about the *y* axis, then repositions to its original location; 52–65 s, DI and DIII fade in, DI and DII fade out, then DIII orientates to enable visualization of ^{781}FPNG^{784} and the ^{724}CXXC^{727} motif; 65–77 s, C647, C703, ^{724}CXXC^{727}, T751, and ^{781}FPNG^{784} appear sequentially in purple and red space fill; 77–86 s, DIII rotates about the *y* axis, then repositions to its original location; 86–101 s, DI and DII fade in, then the entire gH molecule, with all of the mutations mapped, rotates around the *y* axis.

Movie S1

Other Supporting Information Files

Table S1 (DOC)
Table S2 (DOC)
Table S3 (DOC)